

A cross-platform transcriptomic risk score integrating LymphoMAP microenvironment archetypes and immune evasion-associated programs in diffuse large B-cell lymphoma

XIAOCHANG CHEN, JIN ZHANG, SHENHE JIN, LUQIAO WANG and YE ZHANG

Department of Hematology, Sir Run Run Shaw Hospital, Zhejiang University School of Medicine, Hangzhou, Zhejiang 310016, P.R. China

Received February 12, 2026; Accepted April 14, 2026

DOI: 10.3892/ol.2026.15681

Abstract. Diffuse large B-cell lymphoma (DLBCL) is clinically heterogeneous and existing prognostic indices incompletely capture its biological diversity. The present study aimed to investigate how transcriptome-inferred LymphoMAP archetypes (lymph node-like, fibroblast-macrophage-rich and T cell-exhausted) relate to genetic subtypes and immune evasion-associated programs, and whether integrating these dimensions improves risk stratification beyond the International Prognostic Index (IPI). Using the DLBCL-2018 cohort (n=562), LymphoMAP archetypes were inferred and immune programs were quantified by single-sample gene set enrichment analysis, summarizing them into an immune evasion-associated index. In the immunochemotherapy-treated subset (n=234), overall survival was assessed and an elastic-net Cox model was developed to derive a transcriptomic risk score (RScore-Expr). The score was externally evaluated in four independent Gene Expression Omnibus cohorts (n=1,173) with a random-effects meta-analysis performed across studies. LymphoMAP archetypes were non-randomly associated with genetic subtypes ($\chi^2=20.85$, $P=0.0076$) and exhibited distinct immune-program patterns. While archetypes alone were not prognostic in the treated subset (log-rank $P=0.67$), an integrated model identified high-risk patients (log-rank $P=0.0026$) with modest discrimination (C-index: 0.624; time-dependent area under the curve values: 0.662/0.628/0.642 at 12/36/60 months). When added to the IPI, the score improved corrected discrimination (0.639 to 0.687), improved model fit (likelihood-ratio $\chi^2=12.32$, $P=4.48 \times 10^{-4}$), and yielded higher net benefit on decision-curve analysis at 24 and 60 months. In external cohorts, RScore-Expr showed a consistent association with survival (pooled hazard ratio per 1 standard deviation,

1.13; 95% confidence interval 1.01-1.26; $P=0.033$). These results support a cross-platform framework linking microenvironment archetypes, immune evasion-associated programs and tumor genetics. The novelty of the current study lies in integrating these features into an externally evaluated transcriptomic risk score and formally demonstrating added value beyond the IPI in DLBCL.

Introduction

Diffuse large B-cell lymphoma (DLBCL) accounts for 25-30% of cases of adult non-Hodgkin lymphoma and remains a leading cause of lymphoma-related mortality. Standard first-line immunochemotherapy with rituximab plus cyclophosphamide, doxorubicin, vincristine and prednisone (R-CHOP) cures a substantial proportion of patients; however, 30-40% of patients relapse or develop refractory disease and face poor outcomes (1,2). Clinical indices, including the International Prognostic Index (IPI), remain essential for initial risk stratification but currently do not fully capture the biological drivers of treatment failure (3).

Gene expression profiling (GEP) established the cell-of-origin (COO) concept, and identified activated B-cell-like (ABC) and germinal center B-cell-like (GCB) DLBCL subgroups with distinct biological characteristics and outcomes (4,5). Although immunohistochemistry-based algorithms (such as the Hans classifier) have enabled broader adoption of COO assignment in routine clinical practice, COO alone cannot encompass the full spectrum of transcriptomic heterogeneity (6). Subsequent GEP studies have uncovered additional programs reflecting host inflammatory response and stromal remodeling, highlighting the contribution of the lymphoma microenvironment (LME) to clinical behavior and therapeutic response (7,8).

Large-scale genomic studies have further refined DLBCL taxonomy by defining recurrent genetic subtypes (including BN2, MCD, N1 and EZB) characterized by distinct oncogenic dependencies and clinical trajectories (9,10). Probabilistic classification tools now support subtype calls in individual tumors, facilitating translational studies and molecularly stratified trials (11). Integrative driver analyses underscore the breadth of genetic heterogeneity, and reinforce the need to combine tumor-intrinsic and microenvironmental features for risk modeling (12). These molecular insights are increasingly

Correspondence to: Professor Ye Zhang, Department of Hematology, Sir Run Run Shaw Hospital, Zhejiang University School of Medicine, 3 Qingchun East Road, Hangzhou, Zhejiang 310016, P.R. China
E-mail: zhangye0929@zju.edu.cn

Key words: diffuse large B-cell lymphoma, microenvironment, immune evasion, LymphoMAP, prognostic model, transcriptome

reflected in modern disease frameworks, including the revised World Health Organization classification of lymphoid neoplasms (13).

Beyond tumor-intrinsic alterations, the LME shapes immune surveillance, therapy response and resistance. Transcriptome-based approaches that model LME states have revealed reproducible microenvironment-defined DLBCL subtypes with distinct cellular compositions and outcomes (14). However, a practical cross-platform framework linking LME states with tumor genetics, immune evasion programs and clinical risk remains incomplete.

Recently, LymphoMAPs have described three recurring LME archetypes: Lymph node-like (LN), fibroblast-macrophage-rich (FMAC) and T cell-exhausted (TEX), capturing orthogonal axes of immune and stromal remodeling across B-cell lymphomas (15). These archetypes offer an interpretable lens to assess LME states from bulk transcriptomes and suggest therapeutic hypotheses; however, their relationship with established genetic subtypes and their prognostic value in immunochemotherapy-treated DLBCL remain incompletely defined.

DLBCL can evade immune elimination through diverse mechanisms, including impaired antigen presentation and loss of co-stimulatory signals; notably, combined inactivation of β 2-microglobulin and CD58 provides a canonical genetic route to escape T and natural killer cell-mediated killing (16). The present study hypothesized that quantifying immune evasion programs in parallel with LymphoMAP archetype inference may improve biological interpretation and help identify clinically relevant risk states in DLBCL.

Accordingly, the present study aimed to investigate the relationships of transcriptome-inferred LymphoMAP archetypes with DLBCL genetic subtypes and immune evasion-associated transcriptional programs, to derive an immune evasion-associated index (IEAI), to assess the prognostic value of these features in immunochemotherapy-treated patients, to develop and externally evaluate a cross-platform transcriptomic risk score (RScore-Expr), and to examine whether this score adds prognostic information beyond the IPI.

Materials and methods

Study design and cohorts. The present retrospective study integrated publicly available transcriptomic, genomic and clinical data. The full DLBCL-2018 cohort (n=562) was obtained from the National Cancer Institute (NCI) Genomic Data Commons publication page for 'Genetics and Pathogenesis of Diffuse Large B-Cell Lymphoma' (<https://gdc.cancer.gov/about-data/publications/DLBCL-2018>) and the corresponding published study (17), using the public log₂-normalized RNA-seq expression matrix (RNAseq_gene_expression_562.txt) together with the matched clinical and molecular annotations provided in Supplementary Appendix 2 of the published DLBCL-2018 study. External validation was performed using four independent DLBCL cohorts from the Gene Expression Omnibus (GEO; <https://www.ncbi.nlm.nih.gov/geo/>): GSE10846 (8), GSE31312 (18), GSE32918 (19) and GSE87371 (20). The overall study design and analytical workflow are summarized in Fig. 1.

Ethics statement. All analyses were performed on de-identified, publicly available datasets. According to local regulations, institutional review board approval and informed consent were not required for the present study.

Transcriptomic data processing. For DLBCL-2018 data, gene-level expression was analyzed using the log₂-normalized expression matrix provided in the public DLBCL-2018 release together with the matched clinical and molecular sample annotations. For the external GEO validation cohorts, processed expression matrices obtained from the GEO were used for transcriptomic analyses; GEO data retrieval and handling were performed in R (version 4.4.1; R Foundation for Statistical Computing, Vienna; <https://www.r-project.org/>) using the GEOquery R package (version 2.78.0; <https://bioconductor.org/packages/GEOquery/>). Probe sets were mapped to gene symbols using platform annotations and multiple probes mapping to the same gene were aggregated by median expression. For cross-platform modeling, predictors were aligned by gene symbol across cohorts. Predictor values were then scaled using the mean and standard deviation (SD) of the discovery cohort, defined as the immunochemotherapy-treated NCI Center for Cancer Research (NCICCR) subset with overall survival (OS) data available (n=234).

LymphoMAP archetype inference. The LymphoMAP archetypes LN, FMAC and TEX were inferred from bulk gene expression using the published LymphoMAP framework (17). Each sample was assigned to the archetype with the highest posterior probability.

Immune program scoring and IEAI. Immune programs were quantified using single-sample gene set enrichment analysis, implemented through gene set variation analysis (GSVA) using the GSVA R package (version 1.52.3) (21,22). Gene sets were curated from the Molecular Signatures Database hallmark collection using the msgdbr R package (version 25.1.1; <https://CRAN.R-project.org/package=msgdbr>) and from published immune signatures capturing antigen presentation (MHC class I and II), cytolytic activity, T-cell exhaustion, myeloid suppression, interferon- γ response and TGF- β signaling (23). Signature scores were centered and scaled. An IEAI was defined to summarize the balance between immune-suppressive and immune-recognition programs, and is interpreted here as an immune evasion-associated transcriptional phenotype rather than direct genomic proof of immune escape: $IEAI = z [(Exhaustion + MyeloidSuppression + TGF-\beta) - (MHC-I + MHC-II + Cytolytic)]$, where z indicates standardization within the discovery cohort; a higher IEAI indicates a more immune-suppressed/antigen-presentation-low transcriptional state. For gene-level comparisons, IEAI-high and IEAI-low cases were defined as the upper and lower tertiles of the IEAI distribution, respectively, and samples in the middle tertile were excluded from the two-group analysis. Gene-level expression differences for TAP1, TAP2, B2M, HLA-A, HLA-B, HLA-C, CIITA and CD58 between IEAI-high and IEAI-low cases were assessed using the Wilcoxon rank-sum test.

Public data access and preprocessing tools. Public microarray datasets were obtained from GEO under accession numbers

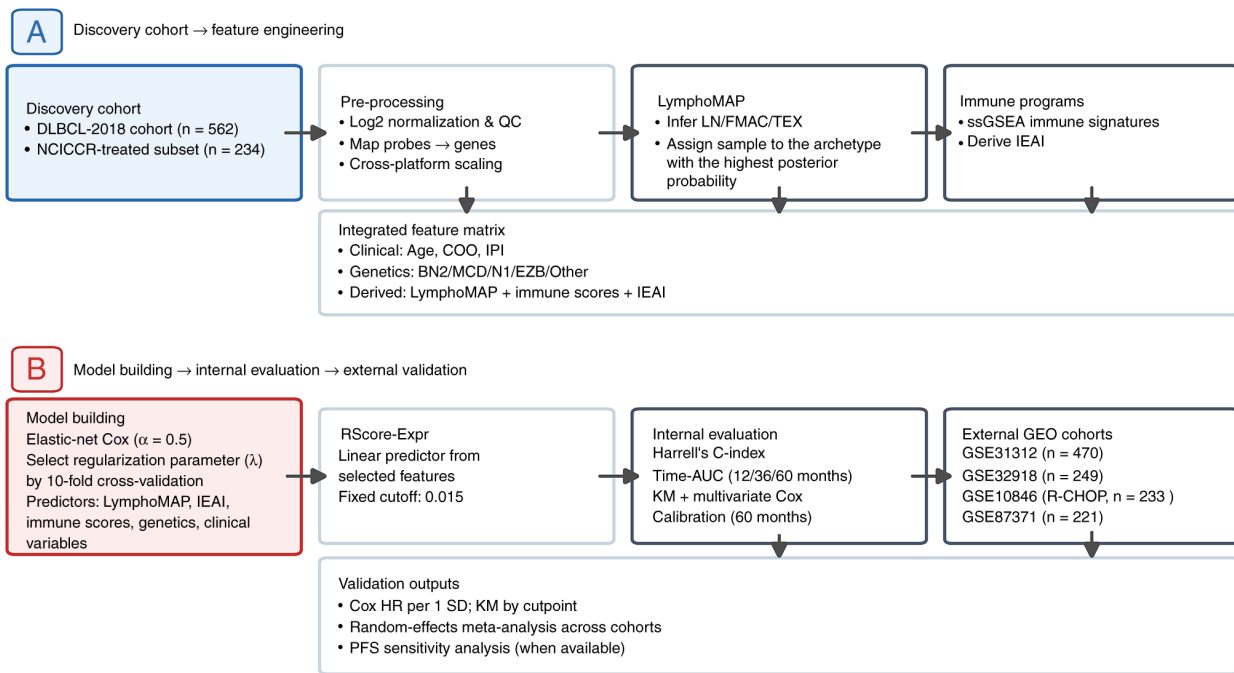


Figure 1. Study design and analytical workflow. (A) Discovery-cohort feature engineering. The full DLBCL-2018 cohort (n=562) was used for transcriptomic, genomic and microenvironment association analyses, including LymphoMAP inference, immune-program scoring and derivation of the IEAI. The frontline immunochemotherapy-treated NCICCR subset (n=234) was used as the discovery cohort for prognostic modeling. (B) Model development, internal evaluation and external validation. An elastic-net Cox model ($\alpha=0.5$) with 10-fold cross-validation was used to select the regularization parameter (λ) and derive the transcriptomic risk score (RScore-Expr). Internal evaluation included Harrell's C-index, time-dependent AUC, KM analysis, multivariate Cox regression and calibration. External validation was performed in four independent GEO cohorts using continuous HR per 1 SD increase in RScore-Expr, random-effects meta-analysis and PFS sensitivity analysis where available. AUC, area under the curve; COO, cell-of-origin; DLBCL, diffuse large B-cell lymphoma; FMAC, fibroblast-macrophage-rich; GEO, Gene Expression Omnibus; HR, hazard ratio; IEAI, immune evasion-associated index; IPI, International Prognostic Index; KM, Kaplan-Meier; LN, lymph node-like; NCICCR, National Cancer Institute Center for Cancer Research; PFS, progression-free survival; R-CHOP, rituximab plus cyclophosphamide, doxorubicin, vincristine and prednisone; SD, standard deviation; ssGSEA, single-sample gene set enrichment analysis; TEX, T cell-exhausted; QC, quality control.

GSE10846, GSE31312, GSE32918 and GSE87371. When batch effects were suspected in cross-cohort exploratory analyses, empirical Bayes adjustment (ComBat) was used as a sensitivity analysis (24). Where differential expression screening was required, linear modeling with empirical Bayes moderation was performed using limma R package (version 3.60.6) (25). Cohort-level mutation and homozygous deletion frequencies for selected antigen-presentation and immune evasion-associated genes were extracted from the previously published appendix-level genomic summaries of the DLBCL-2018 resource, and are presented descriptively as genomic context only; no sample-level enrichment analysis by IEAI stratum was performed.

Clinical and molecular covariates. Baseline clinical variables (age, sex and treatment category) were extracted from the provided clinical annotations. Ann Arbor stage (26), lactate dehydrogenase (LDH) ratio, Eastern Cooperative Oncology Group (ECOG) performance status (27) and extranodal involvement were also used when available. The primary clinical baseline model used IPI alone. A sensitivity analysis used the individual IPI components (age >60 years, stage III/IV, elevated LDH, ECOG >1 and >1 extranodal site) as the baseline clinical model. COO (ABC vs. GCB) and genetic subtype calls (BN2, MCD, N1, EZB and Other) followed published assignments generated using a probabilistic classifier.

Survival endpoints. OS was defined as time from diagnosis to death from any cause; patients alive at last follow-up were censored. For cohorts with progression-free survival (PFS), PFS was defined as time from diagnosis to progression/relapse or death, with censoring at last follow-up.

Statistical analysis. Associations between categorical variables were assessed using χ^2 or Fisher's exact tests. Differences in continuous variables across archetypes were assessed using the Kruskal-Wallis test for overall group comparisons, as appropriate. No post hoc pairwise comparisons were performed. Survival was analyzed using Kaplan-Meier estimates and compared with the log-rank test. Multivariate Cox proportional hazards models were fitted using the survival R package (version 3.8-3; <https://CRAN.R-project.org/package=survival>) to estimate hazard ratios (HRs) and 95% confidence intervals (CIs); proportional hazards assumptions were evaluated using Schoenfeld residuals. Associations between the IEAI and ESTIMATE-derived tumor purity, stromal score, immune score and ESTIMATEScore were assessed using Spearman correlation coefficients. ESTIMATE-based stromal (28), immune and purity scores were calculated using the estimate R package (version 1.0.13; <https://bioinformatics.mdanderson.org/estimate/rpackage.html>) in sensitivity analyses to assess whether bulk immune scores primarily reflected tumor purity or microenvironment abundance. All statistical tests were two-sided, and $P < 0.05$ was considered to indicate a

statistically significant difference unless otherwise specified. For multiple testing in gene-level expression comparisons, Benjamini-Hochberg-adjusted Q-values were additionally reported. Figures were generated using the ggplot2 R package (version 4.0.1; <https://cran.r-project.org/package=ggplot2>).

Model development. To integrate microenvironment, immune, genetic and clinical information, an elastic-net penalized Cox model ($\alpha=0.5$) was trained in the NCICCR-treated subset using the glmnet R package (version 4.1-10; <https://CRAN.R-project.org/package=glmnet>). Candidate predictors included LymphoMAP archetype, genetic subtype, IEAI, immune signature scores, COO, age and IPI group. The regularization parameter (λ) was selected by 10-fold cross-validation to maximize the partial likelihood. The resulting linear predictor defined the transcriptomic risk score (RScore-Expr). For visualization, patients were dichotomized at the optimal cutpoint derived in discovery (0.015).

Model performance evaluation. Discrimination was summarized using Harrell's C-index and time-dependent receiver operating characteristic (ROC) curves with area under the curve (AUC) values at 12, 36 and 60 months, using the timeROC R package (version 0.4; <https://CRAN.R-project.org/package=timeROC>). Calibration at 60 months was assessed by comparing predicted and observed survival probabilities using bootstrap resampling. Added clinical utility beyond IPI was evaluated by comparing IPI-only, RScore-Expr-only and IPI + RScore-Expr models using corrected C-indices, likelihood-ratio tests, Akaike information criterion (AIC) and decision-curve analysis at 24 and 60 months. Reporting followed TRIPOD recommendations for prediction model development and validation (30).

External validation and meta-analysis. RScore-Expr was calculated in each external cohort using the discovery model coefficients after feature alignment and scaling. Cox models were fit within each cohort to estimate HRs per 1 SD increase in RScore-Expr. Cohort-specific estimates were summarized using an inverse-variance weighted random-effects meta-analysis; heterogeneity was described using Cochran's Q and I² statistics, but these values were not used to determine model choice. As a complementary analysis, cohort-specific Kaplan-Meier curves were generated using cohort-specific median splits, but the primary external-validation analysis treated RScore-Expr as a continuous predictor.

Results

Patient cohorts and LymphoMAP distribution. The DLBCL-2018 cohort included 562 patients with baseline clinical and transcriptomic data. The median age was 62 years [interquartile range (IQR) 52-70], and 242/562 (43.1%) of patients were female. LymphoMAP archetypes were inferred for all cases, with 179 (31.9%) classified as LN, 227 (40.4%) as FMAC and 156 (27.8%) as TEX. The distribution of genetic subtypes across the full cohort was: BN2, 98 (17.4%); EZB, 68 (12.1%); MCD, 68 (12.1%); N1, 18 (3.2%); and Other, 310 (55.2%) (Table SI).

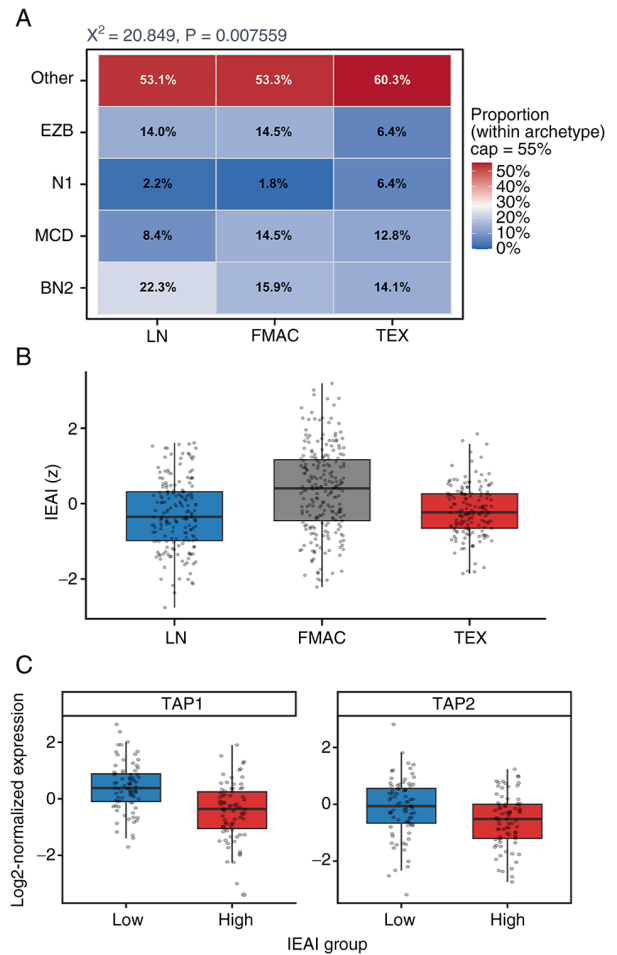


Figure 2. LymphoMAP archetypes are associated with genetic subtypes and IEAI. (A) Heatmap showing the distribution of genetic subtypes across LymphoMAP archetypes in the diffuse large B-cell lymphoma-2018 cohort. The association was significant as determined by χ^2 test ($\chi^2=20.849$; $P=0.007559$). (B) Distribution of the IEAI across LymphoMAP archetypes. The y-axis shows IEAI (z), where z denotes the standardized IEAI score (z-score). FMAC showed the highest IEAI value, whereas TEX overlapped substantially with LN, supporting partial but incomplete correspondence between categorical archetype labels and the continuous immune-state score. (C) Representative expression of antigen-processing genes in the discovery cohort stratified by IEAI group. IEAI-high cases showed lower expression of TAP1 and TAP2, supporting an immune evasion-associated transcriptional phenotype centered on impaired antigen-processing/presentation programs. FMAC, fibroblast-macrophage-rich; IEAI, immune evasion-associated index; LN, lymph node-like; TEX, T cell-exhausted.

LymphoMAP archetypes associated with genetic subtypes and IEAI. Genetic subtypes were non-randomly distributed across LymphoMAP archetypes ($\chi^2=20.85$, $P=0.0076$; Fig. 2A). Relative differences were observed across archetypes, with BN2 more frequent in LN, FMAC showing relatively higher proportions of MCD/EZB, and TEX containing a larger fraction of N1/Other cases.

Immune evasion-associated programs, summarized by the IEAI, showed distinct distributions across archetypes (Fig. 2B). LN tumors showed the lowest IEAI values (median, -0.35), FMAC tumors showed the highest values (median, 0.40) and TEX tumors showed intermediate-to-low values (median, -0.23) that were closer to LN than to FMAC, indicating that the categorical LymphoMAP archetypes and the continuous IEAI capture overlapping but non-identical immune states (Fig. 2B; Table SI).

Table I. Baseline characteristics of the discovery immunochemotherapy cohort stratified by RScore-Expr score.

Characteristic	Overall (n=234)	Low RScore-Expr (n=117)	High RScore-Expr (n=117)	P-value
Median age, years (IQR)	61.0 (49.0-72.0)	57.0 (47.0-69.0)	65.0 (54.0-73.0)	0.0019
Sex				1.000
Female	95 (40.6%)	47 (40.2%)	48 (41.0%)	
Male	139 (59.4%)	70 (59.8%)	69 (59.0%)	
Ann Arbor stage				0.793
I-II	109 (46.6%)	56 (47.9%)	53 (45.3%)	
III-IV	122 (52.1%)	60 (51.3%)	62 (53.0%)	
LDH ratio				0.481
≤1	97 (41.5%)	51 (43.6%)	46 (39.3%)	
>1	105 (44.9%)	49 (41.9%)	56 (47.9%)	
ECOG				0.263
0-1	162 (69.2%)	83 (70.9%)	79 (67.5%)	
≥2	50 (21.4%)	21 (17.9%)	29 (24.8%)	
Extranodal sites				0.437
0-1	190 (81.2%)	98 (83.8%)	92 (78.6%)	
>1	30 (12.8%)	13 (11.1%)	17 (14.5%)	
IPI group				0.022
Low	81 (34.6%)	50 (42.7%)	31 (26.5%)	
Low-Intermediate	45 (19.2%)	18 (15.4%)	27 (23.1%)	
High-Intermediate	44 (18.8%)	16 (13.7%)	28 (23.9%)	
High	64 (27.4%)	33 (28.2%)	31 (26.5%)	
COO				<0.001
ABC	82 (35.0%)	22 (18.8%)	60 (51.3%)	
GCB	110 (47.0%)	78 (66.7%)	32 (27.4%)	
Genetic subtype				0.0039
BN2	42 (17.9%)	22 (18.8%)	20 (17.1%)	
MCD	19 (8.1%)	4 (3.4%)	15 (12.8%)	
N1	6 (2.6%)	0 (0.0%)	6 (5.1%)	
EZB	50 (21.4%)	31 (26.5%)	19 (16.2%)	
Other	117 (50.0%)	60 (51.3%)	57 (48.7%)	

Continuous variables are shown as median (IQR), and categorical variables as n (%). P-values were calculated using the Mann-Whitney U test or Fisher's exact/ χ^2 test, as appropriate. High and low transcriptomic risk groups were defined using the prespecified discovery cutoff. ABC, activated B-cell-like; COO, cell-of-origin; ECOG, Eastern Cooperative Oncology Group; GCB, germinal center B-cell-like; IPI, International Prognostic Index; LDH, lactate dehydrogenase.

Exploratory expression analyses in the discovery cohort further showed reduced TAP1 ($P=1.63 \times 10^{-7}$; $Q=1.31 \times 10^{-6}$) and TAP2 ($P=0.0030$; $Q=0.0122$) expression in IEAI-high cases, defined as the upper tertile of the IEAI distribution, compared with IEAI-low cases defined as the lower tertile (Fig. 2C; Table SII); samples in the middle tertile were excluded from this two-group comparison. TAP1 and TAP2 encode key components of the transporter associated with antigen processing and are central to MHC class I antigen presentation; thus, their reduced expression is consistent with an immune evasion-associated state marked by impaired antigen processing/presentation (31).

LymphoMAP archetypes are not independently prognostic in immunochemotherapy-treated patients. The current study subsequently focused on the NCICCR-treated subset

with immunochemotherapy and OS data (n=234). Baseline clinical and molecular characteristics of this discovery cohort are summarized in Table I. In this clinically treated subset, LymphoMAP archetypes alone did not stratify OS (log-rank $P=0.67$; Fig. 3A).

In a multivariate Cox model including LymphoMAP archetype, genetic subtype, IEAI, COO, age and IPI group (Table SIII; Fig. 3B), the MCD and N1 genetic subtypes, ABC COO and increasing age were associated with inferior OS, whereas neither FMAC or TEX archetypes nor the IEAI were independently associated with OS.

Development and internal performance of an integrated transcriptomic risk score (RScore-Expr). To integrate microenvironment and immune programs with clinical and

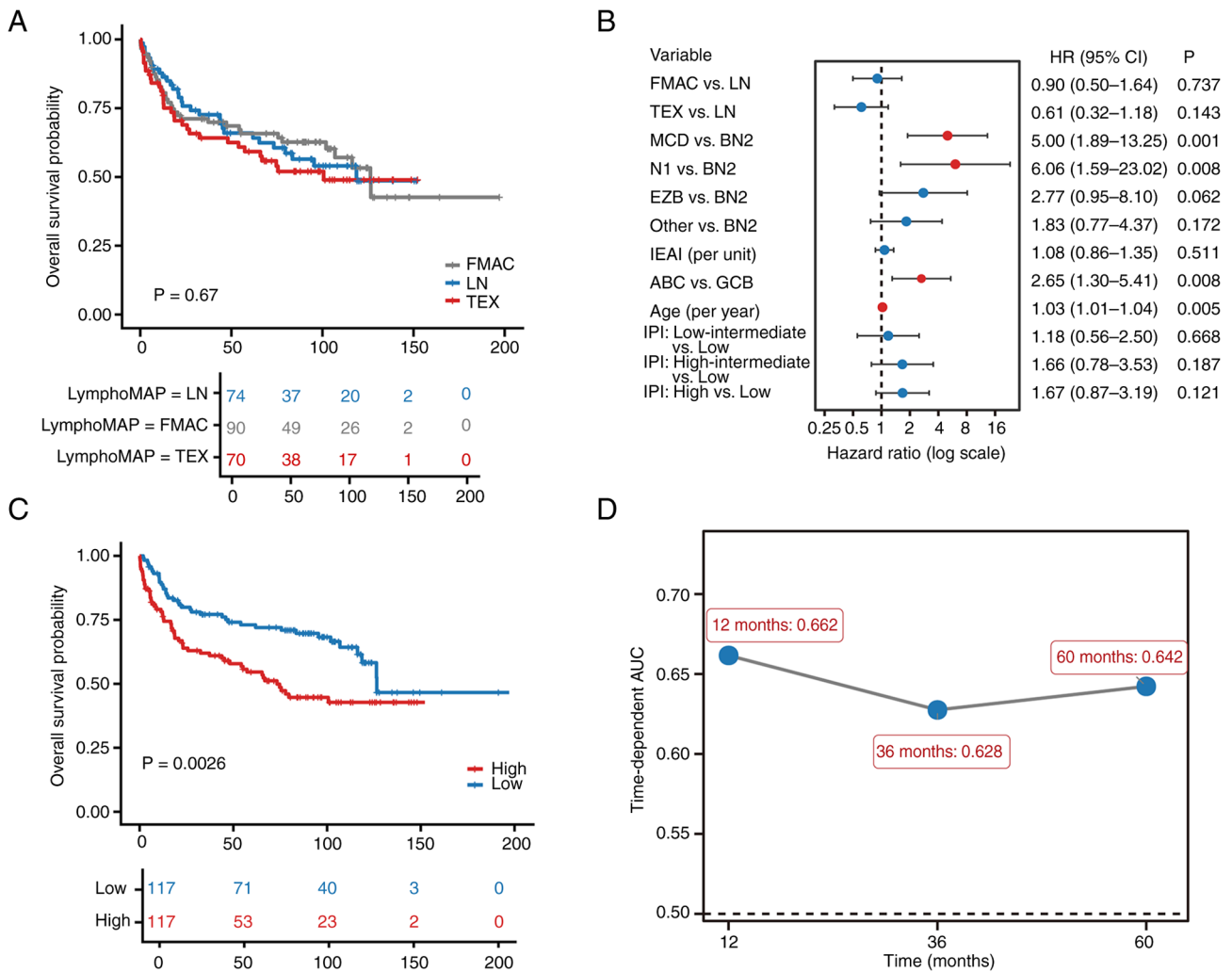


Figure 3. Discovery-cohort prognostic analyses. (A) Kaplan-Meier OS curves for the National Cancer Institute Center for Cancer Research -treated discovery cohort stratified by LymphoMAP archetype, showing no significant separation (log-rank $P=0.67$). (B) Multivariate Cox regression including LymphoMAP archetype, genetic subtype, IEAI, COO, age and IPI group. MCD and N1 genetic subtypes, ABC COO and increasing age were associated with inferior OS, whereas neither FMAC archetype, TEX archetype or IEAI were independently associated with OS. (C) Kaplan-Meier OS curves stratified by high-RScore-Expr versus low-RScore-Expr using the prespecified discovery cutpoint, showing a significant difference (log-rank $P=0.0026$). (D) Time-dependent AUC values of RScore-Expr at 12, 36 and 60 months. ABC, activated B-cell-like; AUC, area under the curve; COO, cell-of-origin; FMAC, fibroblast-macrophage-rich; GCB, germinal center B-cell-like; IEAI, immune evasion-associated index; IPI, International Prognostic Index; LN, lymph node-like; OS, overall survival; TEX, T cell-exhausted.

molecular features, an elastic-net Cox model was trained in the NCICCR-treated subset, yielding a transcriptomic risk score (RScore-Expr). Using the discovery cutpoint (0.015), RScore-Expr stratified patients into high- and low-risk groups with distinct survival outcomes (log-rank $P=0.0026$; Fig. 3C).

RScore-Expr demonstrated moderate discrimination in the treated subset (C-index 0.624). Time-dependent AUC values were 0.662, 0.628 and 0.642 at 12, 36 and 60 months, respectively (Fig. 3D). Modeled continuously, higher RScore-Expr was associated with increased hazard of death (HR per 1 SD, 1.52; 95% CI 1.21–1.89; $P=2.5 \times 10^{-4}$), with an approximately monotonic risk increase across the score range. Calibration at 60 months showed reasonable agreement between predicted and observed survival (Fig. 4D).

Added value of RScore-Expr beyond IPI and clinical utility in the discovery cohort. The present study next compared the transcriptomic model directly against the IPI. In the discovery

cohort, the IPI-only model had a corrected C-index of 0.639, the RScore-Expr-only model had a corrected C-index of 0.624, and the combined IPI + RScore-Expr model improved the corrected C-index to 0.687. Adding RScore-Expr to IPI improved model fit (likelihood-ratio $\chi^2=12.32$, $P=4.48 \times 10^{-4}$) and reduced the AIC from 967.36 to 957.04 (Table II; Fig. 4A). Decision-curve analysis further showed that the combined model provided higher net benefit than either model alone across clinically relevant threshold ranges at both 24 and 60 months (Fig. 4B and C). A sensitivity analysis using the individual IPI components as the clinical baseline yielded concordant results (Table II).

External validation across independent cohorts. RScore-Expr was applied to four independent GEO cohorts (GSE31312, $n=470$; GSE32918, $n=249$; GSE10846, $n=233$; GSE87371, $n=221$; total $n=1,173$). Across the four external cohorts, all cohort-specific HRs for OS were directionally >1 ,

Table II. Comparison of clinical and transcriptomic prognostic models in the discovery cohort.

Model	Corrected C-index	AIC	LR test vs. baseline
Primary analysis			
IPI-only	0.639	967.36	-
RScore-Expr-only	0.624	970.59	-
IPI + RScore-Expr	0.687	957.04	$\chi^2=12.32$; $P=4.48 \times 10^{-4}$
Sensitivity analysis			
IPI components-only	0.687	951.83	-
IPI components +RScore-Expr	0.707	945.33	$\chi^2=8.50$; $P=0.00354$

In the primary analysis, the clinical baseline was IPI-only, whereas the IPI components model was the baseline in the sensitivity analysis. All models were fitted in the same discovery cohort (n=234) with 98 overall survival events. Corrected C-index values are reported so that higher values indicate better discrimination. LR test vs. baseline indicates the likelihood-ratio comparison of each combined model with the corresponding baseline nested Cox model. AIC, Akaike information criterion; IPI, International Prognostic Index; LR, likelihood ratio.

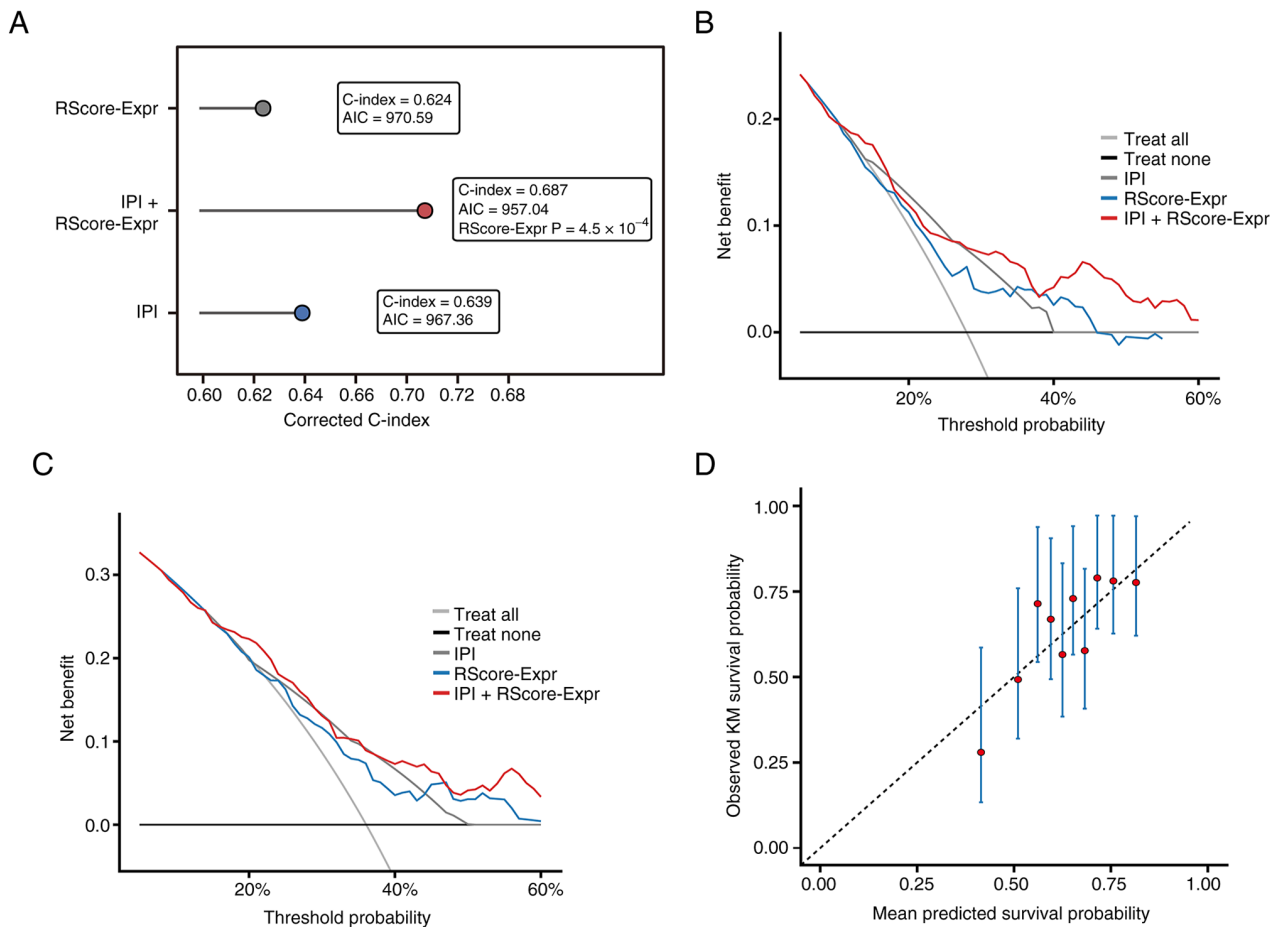


Figure 4. Added value of RScore-Expr beyond IPI and clinical utility in the discovery cohort. (A) Comparison of IPI-only, RScore-Expr-only and IPI + RScore-Expr models. Adding RScore-Expr to IPI improved corrected discrimination (C-index 0.639 to 0.687), reduced AIC and improved model fit (likelihood-ratio $P=4.5 \times 10^{-4}$). Decision-curve analyses for (B) 24-month and (C) 60-month overall survival. Across multiple clinically relevant threshold ranges, the combined IPI + RScore-Expr model yielded higher net benefit than either model alone. (D) Calibration plot comparing mean predicted and observed KM 60-month survival probabilities in the discovery cohort. AIC, Akaike information criterion; IPI, International Prognostic Index; KM, Kaplan-Meier.

indicating a consistent trend toward worse survival with higher RScore-Expr, although none of the individual cohort-specific estimates reached statistical significance. The strongest trends were observed in GSE10846 (HR per 1 SD, 1.27; 95% CI, 0.98-1.65; $P=0.0733$) and GSE32918 (HR, 1.17; 95%

CI, 0.99-1.38; $P=0.0629$), whereas the effect was minimal in GSE31312 (HR, 1.01; 95% CI, 0.87-1.17; $P=0.9302$) and directionally similar but less precise in GSE87371 (HR, 1.24; 95% CI, 0.93-1.63; $P=0.1385$). When summarized using a random-effects meta-analysis, the pooled association for

OS was statistically significant (HR per 1 SD, 1.13; 95% CI, 1.01-1.26; $P=0.0328$; Fig. 5A; Table SIV). Fig. 5B shows the cohort-specific C-index values for OS in the external cohorts, indicating modest but directionally consistent discrimination across datasets.

For PFS, the direction of effect was similar across the cohorts with available data, although neither cohort-specific estimate reached statistical significance (GSE31312, $P=0.2664$; GSE87371, $P=0.0528$). The pooled random-effects association also did not reach statistical significance (HR, 1.14; 95% CI, 0.99-1.31; $P=0.0716$; Table SV). The dichotomized Kaplan-Meier plots shown in Fig. S1 are provided as complementary visualizations, whereas calibration plots for the external continuous models are shown in Fig. S2. Additional supplementary analyses of antigen-processing and immune evasion-associated genes are summarized in Tables SV and SVI. The corresponding statistical comparisons, P-values and Q-values are reported in Table SII.

In the all-cohort analysis, IEAI-high cases showed the strongest reductions in TAP1 and TAP2, together with lower CIITA and HLA-A/B/C expression. In the NCICCR-treated immunochemotherapy discovery cohort ($n=234$), TAP1 and TAP2 showed the most robust differences, whereas the remaining genes showed directionally similar but less stable differences after multiple-testing correction. Cohort-level mutation and homozygous deletion frequencies of selected antigen-presentation and immune evasion-associated genes are summarized in Table SVI as descriptive genomic context. ESTIMATE-based sensitivity analyses showed that the IEAI was only weakly inversely correlated with estimated tumor purity in both the full cohort (Spearman $\rho=-0.142$; $P=7.7\times 10^{-4}$) and the discovery cohort ($\rho=-0.160$; $P=0.014$), whereas the relationship with stromal score was stronger (full cohort: $\rho=0.327$; $P=2.25\times 10^{-15}$; discovery cohort: $\rho=0.370$; $P=6.8\times 10^{-9}$) (Fig. S3; Table SVII). In minimal multivariate Cox models, adding estimated tumor purity did not materially alter the associations of the main predictors with OS, and tumor purity itself was not independently associated with OS (Table SVIII). In a nested model comparison, a likelihood-ratio test comparing Cox models with and without tumor purity showed that adding tumor purity to the minimal OS Cox model did not improve model fit ($\chi^2=0.157$, 1 degree of freedom, $P=0.6922$). The corresponding gene-level expression patterns are visualized in Fig. S4.

Discussion

This integrative analysis linked transcriptome-inferred LME archetypes, tumor genetic subtypes and immune evasion-associated programs in DLBCL, and proposed a cross-platform transcriptomic risk score (RScore-Expr). In the DLBCL-2018 cohort, LymphoMAP archetypes were associated with genetic subtypes and displayed distinct immune-program patterns. While archetypes alone were not prognostic in the immunochemotherapy-treated subset, an integrated model yielded a risk score with moderate internal discrimination, added value beyond IPI and a statistically supported, albeit modest, association with survival across four external cohorts.

The biological associations between genetic subtype and microenvironment state remain plausible. ABC-type DLBCL

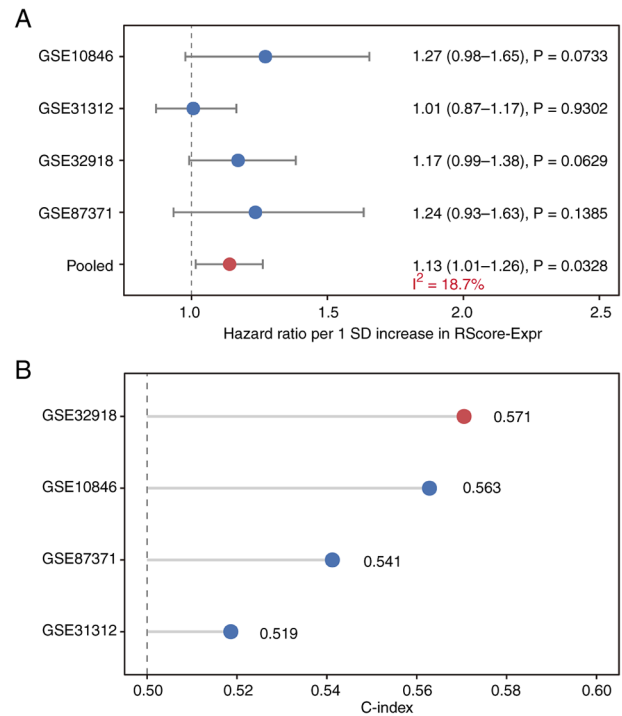


Figure 5. External validation of RScore-Expr across independent Gene Expression Omnibus cohorts. (A) Forest plot summarizing cohort-specific and pooled hazard ratios for overall survival per 1 SD increase in RScore-Expr across four external cohorts. The pooled random-effects estimate was 1.13 (95% confidence interval 1.01-1.26; $P=0.0328$), with $I^2=18.7\%$. (B) Cohort-specific C-index values for overall survival in the external cohorts, showing modest but directionally consistent discrimination. SD, standard deviation.

and MCD tumors are frequently characterized by chronic active B-cell receptor signaling and oncogenic MYD88 signaling, which can shape inflammatory cytokine production and immune interactions (10,32,33). These pathways are therapeutically actionable; an early-phase study of Bruton tyrosine kinase inhibition (ibrutinib) demonstrated the feasibility of molecularly informed targeting in DLBCL, and motivate integration of tumor-intrinsic and microenvironmental biomarkers (34).

Across the full cohort, the LN archetype exhibited the lowest IEAI, whereas FMAC showed the highest values and TEX overlapped substantially with LN, indicating that the IEAI is related to, but not equivalent to, categorical LymphoMAP labels. The IEAI used in the present study was designed to summarize opposing immune forces by contrasting exhaustion/myeloid suppression/TGF- β activity with antigen presentation and cytolytic programs; TEX remains biologically consistent with a TEX state, a well-characterized form of T-cell dysfunction arising from persistent antigen stimulation and inhibitory receptor signaling (35). Cytolytic activity signatures have been linked to tumor immunogenicity and immune engagement across multiple cancer types, including melanoma, lung cancer and colorectal cancer (36).

Inferring LME states from bulk transcriptomes is necessarily indirect. Nevertheless, prior work has shown that bulk expression contains sufficient information to estimate immune and stromal composition; for example, deconvolution approaches such as CIBERSORT enable robust enumeration of

cell subsets from tissue expression profiles (37). In the current ESTIMATE-based sensitivity analyses, the IEAI showed only a weak inverse correlation with estimated tumor purity in both the full cohort ($\rho=-0.142$) and the discovery cohort ($\rho=-0.160$), whereas the relationship with stromal score was stronger ($\rho=0.327$ and 0.370 , respectively), supporting that IEAI reflects bulk microenvironment composition rather than purity alone. Moreover, adding tumor purity to the minimal OS model did not materially alter the estimated effects of the main predictors, and tumor purity itself was not independently associated with outcome. The FMAC archetype, in particular, may reflect fibroblast-macrophage interactions, and stromal remodeling that can physically and functionally restrict effector lymphocyte infiltration. Notably, TGF- β signaling can contribute to immune exclusion and attenuate responses to PD-1 or PD-L1 blockade by limiting T-cell access to tumor nests (38). These mechanistic considerations align with the cancer-immunity cycle framework, where impairments in antigen presentation, priming, trafficking and effector function can converge to create immunologically 'cold' or resistant phenotypes (39).

Although RScore-Expr improved risk stratification in the discovery cohort, external validation highlighted a common challenge for transcriptome-derived prognostic models: Effect sizes are often attenuated across heterogeneous cohorts and measurement platforms. Therefore RScore-Expr was evaluated as a continuous predictor (per 1 SD increase) and the results were summarized by inverse-variance random-effects meta-analysis to account for between-cohort heterogeneity. Meta-analytic approaches provide a principled framework to combine cohort-specific HRs and to quantify heterogeneity (40,41). The modest pooled HR observed in the current study suggested that RScore-Expr may capture a component of risk that is reproducible but not dominant, consistent with the fact that outcome under R-CHOP is influenced by multiple factors, including IPI-related clinical risk, COO, genetic subtype, and other host- and disease-related features. Several considerations are important for interpretation. First, median-splitting the score within individual cohorts did not consistently yield statistically significant separation, despite directionally consistent trends. This is expected because dichotomizing continuous predictors can reduce statistical power and obscure risk gradients, particularly when cohort sizes are modest and baseline risk differs across datasets (42). Second, the treated subset used for model development was of moderate size, and the model may still be susceptible to overfitting despite regularization. General guidance on multivariate prognostic modeling emphasizes careful internal validation, calibration assessment and the need for external validation before clinical application (43). The current study followed TRIPOD reporting principles to facilitate transparent interpretation and replication (30). A limitation of the current study is that direct sample-to-sample concordance testing against the original published LymphoMAP calls was not performed, and pretreatment tumor transcriptomic data from CAR T-treated DLBCL were not available for validation. Biologically, the present results support the view that immune evasion-associated programs and microenvironment remodeling are integral components of malignant progression. Expression analyses in IEAI-high cases highlighted reduced TAP1/TAP2 and related antigen-processing signals, supporting

an immune evasion-associated transcriptional phenotype. However, publicly available appendix-level genomic summaries did not allow direct sample-level enrichment testing of HLA/B2M-related lesions by IEAI status. Immune evasion and tumor-microenvironment crosstalk are increasingly recognized as enabling capabilities in cancer biology (44). In the era of immunotherapy, immune evasion-associated programs, impaired antigen-processing/presentation signals and tumor-microenvironment crosstalk may also help explain interpatient variability in response to emerging strategies in lymphoma. Immune checkpoint blockade has become a central modality in cancer therapy and is being actively explored in aggressive lymphoma, particularly in rational combinations (45).

Future work should focus on prospective validation and on refining the score for clinical deployment, including robust cross-platform normalization, harmonized endpoint definitions and incorporation of additional modalities (for example, circulating tumor DNA, spatial profiling or single-cell data). Notably, any clinical implementation should preserve the continuous nature of the score and pre-specify cutpoints to avoid optimistic bias. Dedicated validation in pretreatment tumor-bulk datasets from CAR T-treated DLBCL would be particularly valuable. The broader field of checkpoint blockade and combination immunotherapy continues to evolve, and integrating microenvironment archetypes with tumor genetics may help guide personalized immunomodulatory approaches (46).

In conclusion, LymphoMAP archetypes were revealed to be biologically linked to DLBCL genetic subtype structure and to an immune evasion-associated transcriptional axis, but were not independently prognostic in the treated subset. The novelty of the current study lies in integrating microenvironment archetypes, an immune evasion-associated transcriptional index, genetic subtypes and clinical variables into a single cross-platform transcriptomic risk model that was externally evaluated across independent cohorts and benchmarked against IPI. This integrated framework identifies a modest but reproducible risk signal and provides a more interpretable basis for future molecular risk stratification in DLBCL.

Acknowledgements

Not applicable.

Funding

No funding was received.

Availability of data and materials

The data generated in the present study may be requested from the corresponding author.

Authors' contributions

XC wrote the original draft, performed the formal analyses, curated and harmonized the publicly available clinical, transcriptomic and genomic datasets, and contributed to

study conceptualization. YZ contributed to study conceptualization, supervised the analytical methodology and investigation, and critically revised the manuscript. JZ contributed to acquisition and organization of the publicly available datasets, review of the analytical results and critical revision of the manuscript. SJ contributed to interpretation of the results, review of the analytical framework, figure preparation based on the analytical findings and critical revision of the manuscript. LW contributed to study design refinement, interpretation of the results, methodological review and critical revision of the manuscript. XC and YZ confirm the authenticity of all the raw data. All authors read and approved the final manuscript.

Ethics approval and consent to participate

Not applicable.

Patient consent for publication

Not applicable.

Competing interests

The authors declare that they have no competing interests.

References

- Vannata B, Conconi A, Winkler J, Cascione L, Casaluci GM, Nassi L, Moia R, Piroso MC, Moccia AA, Stathis A, *et al*: Late relapse in patients with diffuse large B-cell lymphoma: Impact of rituximab on their incidence and outcome. *Br J Haematol* 187: 478-487, 2019.
- Coiffier B and Sarkozy C: Diffuse large B-cell lymphoma: R-CHOP failure-what to do? *Hematology Am Soc Hematol Educ Program* 2016: 366-378, 2016.
- A predictive model for aggressive non-Hodgkin's lymphoma. *N Engl J Med* 329: 987-994, 1993.
- Alizadeh AA, Eisen MB, Davis RE, Ma C, Lossos IS, Rosenwald A, Boldrick JC, Sabet H, Tran T, Yu X, *et al*: Distinct types of diffuse large B-cell lymphoma identified by gene expression profiling. *Nature* 403: 503-511, 2000.
- Rosenwald A, Wright G, Chan WC, Connors JM, Campo E, Fisher RI, Gascoyne RD, Muller-Hermelink HK, Smeland EB, Giltman JM, *et al*: The use of molecular profiling to predict survival after chemotherapy for diffuse large-B-cell lymphoma. *N Engl J Med* 346: 1937-1947, 2002.
- Hans CP, Weisenburger DD, Greiner TC, Gascoyne RD, Delabie J, Ott G, Müller-Hermelink HK, Campo E, Braziel RM, Jaffe ES, *et al*: Confirmation of the molecular classification of diffuse large B-cell lymphoma by immunohistochemistry using a tissue microarray. *Blood* 103: 275-282, 2004.
- Monti S, Savage KJ, Kutok JL, Feuerhake F, Kurtin P, Mihm M, Wu B, Pasqualucci L, Neuberger D, Aguiar RC, *et al*: Molecular profiling of diffuse large B-cell lymphoma identifies robust subtypes including one characterized by host inflammatory response. *Blood* 105: 1851-1861, 2005.
- Lenz G, Wright G, Dave SS, Xiao W, Powell J, Zhao H, Xu W, Tan B, Goldschmidt N, Iqbal J, *et al*: Stromal gene signatures in large-B-cell lymphomas. *N Engl J Med* 359: 2313-2323, 2008.
- Schmitz R, Wright GW, Huang DW, Johnson CA, Phelan JD, Wang JQ, Roulland S, Kasbekar M, Young RM, Shaffer AL, *et al*: Genetics and pathogenesis of diffuse large B-cell lymphoma. *N Engl J Med* 378: 1396-1407, 2018.
- Chapuy B, Stewart A, Dunford AJ, Kim J, Kamburov A, Redd RA, Lawrence MS, Roemer MGM, Li AJ, Ziepert M, *et al*: Molecular subtypes of diffuse large B cell lymphoma are associated with distinct pathogenic mechanisms and outcomes. *Nat Med* 24: 679-690, 2018.
- Wright GW, Huang DW, Phelan JD, Coulibaly ZA, Roulland S, Young RM, Wang JQ, Schmitz R, Morin RD, Tang J, *et al*: A probabilistic classification tool for genetic subtypes of diffuse large B cell lymphoma with therapeutic implications. *Cancer Cell* 37: 551-568.e514, 2020.
- Reddy A, Zhang J, Davis NS, Moffitt AB, Love CL, Waldrop A, Leppä S, Pasanen A, Meriranta L, Karjalainen-Lindsberg ML, *et al*: Genetic and functional drivers of diffuse large B cell lymphoma. *Cell* 171: 481-494.e415, 2017.
- Swerdlow SH, Campo E, Pileri SA, Harris NL, Stein H, Siebert R, Advani R, Ghielmini M, Salles GA, Zelenetz AD and Jaffe ES: The 2016 revision of the World Health Organization classification of lymphoid neoplasms. *Blood* 127: 2375-2390, 2016.
- Kotlov N, Bagaev A, Revuelta MV, Phillip JM, Cacciapuoti MT, Antysheva Z, Svekolkina V, Tikhonova E, Mihecheva N, Kuzkina N, *et al*: Clinical and biological subtypes of B-cell lymphoma revealed by microenvironmental signatures. *Cancer Discov* 11: 1468-1489, 2021.
- Li X, Singhal K, Deng Q, Chihara D, Russler-Germain D, Harkins RA, Henderson J, Arita K, Kizhakeyil A, Sun R, *et al*: Large B cell lymphoma microenvironment archetype profiles. *Cancer Cell* 43: 1347-1364.e1313, 2025.
- Challa-Malladi M, Lieu YK, Califano O, Holmes AB, Bhagat G, Murty VV, Dominguez-Sola D, Pasqualucci L and Dalla-Favera R: Combined genetic inactivation of β 2-Microglobulin and CD58 reveals frequent escape from immune recognition in diffuse large B cell lymphoma. *Cancer Cell* 20: 728-740, 2011.
- Schmitz R, Wright GW, Huang DW, Johnson CA, Phelan JD, Wang JQ, Roulland S, Kasbekar M, Young RM, Shaffer AL, *et al*: Genetics and pathogenesis of diffuse large B-cell lymphoma. *N Engl J Med* 378: 1396-1407, 2018.
- Visco C, Li Y, Xu-Monette ZY, Miranda RN, Green TM, Li Y, Tzankov A, Wen W, Liu WM, Kahl BS, *et al*: Comprehensive gene expression profiling and immunohistochemical studies support application of immunophenotypic algorithm for molecular subtype classification in diffuse large B-cell lymphoma: A report from the International DLBCL Rituximab-CHOP Consortium Program Study. *Leukemia* 26: 2103-2113, 2012.
- Barrans SL, Crouch S, Care MA, Worrillow L, Smith A, Patmore R, Westhead DR, Tooze R, Roman E and Jack AS: Whole genome expression profiling based on paraffin embedded tissue can be used to classify diffuse large B-cell lymphoma and predict clinical outcome. *Br J Haematol* 159: 441-453, 2012.
- Dubois S, Tesson B, Mareschal S, Vially PJ, Bohers E, Ruminy P, Etancelin P, Peyrouze P, Copie-Bergman C, Fabiani B, *et al*: Refining diffuse large B-cell lymphoma subgroups using integrated analysis of molecular profiles. *EBioMedicine* 48: 58-69, 2019.
- Subramanian A, Tamayo P, Mootha VK, Mukherjee S, Ebert BL, Gillette MA, Paulovich A, Pomeroy SL, Golub TR, Lander ES and Mesirov JP: Gene set enrichment analysis: A knowledge-based approach for interpreting genome-wide expression profiles. *Proc Natl Acad Sci USA* 102: 15545-15550, 2005.
- Hänzelmann S, Castelo R and Guinney J: GSEA: Gene set variation analysis for microarray and RNA-seq data. *BMC Bioinformatics* 14: 7, 2013.
- Liberzon A, Birger C, Thorvaldsdóttir H, Ghandi M, Mesirov JP and Tamayo P: The Molecular Signatures Database (MSigDB) hallmark gene set collection. *Cell Syst* 1: 417-425, 2015.
- Johnson WE, Li C and Rabinovic A: Adjusting batch effects in microarray expression data using empirical Bayes methods. *Biostatistics* 8: 118-127, 2007.
- Ritchie ME, Phipson B, Wu D, Hu Y, Law CW, Shi W and Smyth GK: limma powers differential expression analyses for RNA-sequencing and microarray studies. *Nucleic Acids Res* 43: e47, 2015.
- Carbone PP, Kaplan HS, Musshoff K, Smithers DW and Tubiana M: Report of the committee on Hodgkin's disease staging classification. *Cancer Res* 31: 1860-1861, 1971.
- Oken MM, Creech RH, Tormey DC, Horton J, Davis TE, McFadden ET and Carbone PP: Toxicity and response criteria of the Eastern cooperative oncology group. *Am J Clin Oncol* 5: 649-655, 1982.
- Yoshihara K, Shahmoradgoli M, Martínez E, Vegesna R, Kim H, Torres-García W, Treviño V, Shen H, Laird PW, Levine DA, *et al*: Inferring tumour purity and stromal and immune cell admixture from expression data. *Nat Commun* 4: 2612, 2013.
- Heagerty PJ, Lumley T and Pepe MS: Time-dependent ROC curves for censored survival data and a diagnostic marker. *Biometrics* 56: 337-344, 2000.

30. Collins GS, Reitsma JB, Altman DG and Moons KG: Transparent reporting of a multivariable prediction model for individual prognosis or diagnosis (TRIPOD): The TRIPOD statement. *Ann Intern Med* 162: 55-63, 2015.
31. Neefjes J, Jongstra ML, Paul P and Bakke O: Towards a systems understanding of MHC class I and MHC class II antigen presentation. *Nat Rev Immunol* 11: 823-836, 2011.
32. Davis RE, Ngo VN, Lenz G, Tolar P, Young RM, Romesser PB, Kohlhammer H, Lamy L, Zhao H, Yang Y, *et al*: Chronic active B-cell-receptor signalling in diffuse large B-cell lymphoma. *Nature* 463: 88-92, 2010.
33. Ngo VN, Young RM, Schmitz R, Jhavar S, Xiao W, Lim KH, Kohlhammer H, Xu W, Yang Y, Zhao H, *et al*: Oncogenically active MYD88 mutations in human lymphoma. *Nature* 470: 115-119, 2011.
34. Wilson WH, Young RM, Schmitz R, Yang Y, Pittaluga S, Wright G, Lih CJ, Williams PM, Shaffer AL, Gerecitano J, *et al*: Targeting B cell receptor signaling with ibrutinib in diffuse large B cell lymphoma. *Nat Med* 21: 922-926, 2015.
35. Wherry EJ: T cell exhaustion. *Nat Immunol* 12: 492-499, 2011.
36. Rooney MS, Shukla SA, Wu CJ, Getz G and Hacohen N: Molecular and genetic properties of tumors associated with local immune cytolytic activity. *Cell* 160: 48-61, 2015.
37. Newman AM, Liu CL, Green MR, Gentles AJ, Feng W, Xu Y, Hoang CD, Diehn M and Alizadeh AA: Robust enumeration of cell subsets from tissue expression profiles. *Nat Methods* 12: 453-457, 2015.
38. Mariathasan S, Turley SJ, Nickles D, Castiglioni A, Yuen K, Wang Y, Kadel EE III, Koeppen H, Astarita JL, Cubas R, *et al*: TGF β attenuates tumour response to PD-L1 blockade by contributing to exclusion of T cells. *Nature* 554: 544-548, 2018.
39. Chen DS and Mellman I: Oncology meets immunology: The cancer-immunity cycle. *Immunity* 39: 1-10, 2013.
40. DerSimonian R and Laird N: Meta-analysis in clinical trials. *Control Clin Trials* 7: 177-188, 1986.
41. Higgins JP, Thompson SG, Deeks JJ and Altman DG: Measuring inconsistency in meta-analyses. *BMJ* 327: 557-560, 2003.
42. Harrell FE Jr, Lee KL and Mark DB: Multivariable prognostic models: Issues in developing models, evaluating assumptions and adequacy, and measuring and reducing errors. *Stat Med* 15: 361-387, 1996.
43. Hanahan D and Weinberg RA: Hallmarks of cancer: the next generation. *Cell* 144: 646-674, 2011.
44. Topalian SL, Drake CG and Pardoll DM: Immune checkpoint blockade: A common denominator approach to cancer therapy. *Cancer Cell* 27: 450-461, 2015.
45. Gao L and Gross DS: Using genomics and proteomics to investigate mechanisms of transcriptional silencing in *Saccharomyces cerevisiae*. *Brief Funct Genomic Proteomic* 5: 280-288a, 2006.
46. Pardoll DM: The blockade of immune checkpoints in cancer immunotherapy. *Nat Rev Cancer* 12: 252-264, 2012.



Copyright © 2026 Chen et al. This work is licensed under a Creative Commons Attribution-NonCommercial-NoDerivatives 4.0 International (CC BY-NC-ND 4.0) License.